

# The Centers of Early-Type Galaxies with HST II: Empirical Models and Structural Parameters<sup>1</sup>

Yong-Ik Byun<sup>2</sup>

Institute for Astronomy, University of Hawaii, 2680 Woodlawn Dr., Honolulu, HI 96822

Carl J. Grillmair<sup>3</sup>

UCO/Lick Observatory, University of California, Santa Cruz, CA 95064

S. M. Faber

UCO/Lick Observatory, Board of Studies in Astronomy and Astrophysics, University of California, Santa Cruz, Santa Cruz, CA 95064

Edward A. Ajhar

Kitt Peak National Observatory, National Optical Astronomy Observatories,<sup>4</sup>  
P. O. Box 26732, Tucson, AZ 85726

Alan Dressler

The Observatories of the Carnegie Institution of Washington  
813 Santa Barbara St., Pasadena, CA 91101

John Kormendy

Institute for Astronomy, University of Hawaii, 2680 Woodlawn Dr., Honolulu, HI 96822

Tod R. Lauer

Kitt Peak National Observatory, National Optical Astronomy Observatories,<sup>4</sup>  
P. O. Box 26732, Tucson, AZ 85726

Douglas Richstone

Department of Astronomy, University of Michigan, Ann Arbor, MI 48109

Scott Tremaine

Canadian Institute for Theoretical Astrophysics, University of Toronto  
60 St. George St., Toronto, M5S 1A7, Canada

---

<sup>1</sup>Based on observations with the NASA/ESA Hubble Space Telescope, obtained at the Space Telescope Science Institute, which is operated by AURA, Inc., under NASA contract NAS 5-26555.

<sup>2</sup>Present address: Institute of Astronomy, National Central University, Chung-Li, Taiwan 32054, R.O.C.

<sup>3</sup>Present address: Jet Propulsion Laboratory, MS 183-900, 4800 Oak Grove Dr., Pasadena, CA 91109

<sup>4</sup>Operated by AURA under cooperative agreement with the National Science Foundation.

## ABSTRACT

We present a set of structural parameters for the central parts of 57 early-type galaxies observed with the Planetary Camera of the Hubble Space Telescope. These parameters are based on a new empirical law that successfully characterizes the centers of early type galaxies. This empirical law assumes that the surface brightness profile is a combination of two power laws with different slopes  $\gamma$  and  $\beta$  for the inner and outer regions. Conventional structural parameters such as core radius and central surface brightness are replaced by break radius  $r_b$ , where the transition between power-law slopes takes place, and surface brightness  $\mu_b$  at that radius. An additional parameter  $\alpha$  describes the sharpness of the break. The structural parameters are derived using a  $\chi^2$  minimization process applied to the mean surface brightness profiles. The resulting model profiles generally give very good agreement to the observed profiles out to the radius of  $\sim 10''$  imaged by the Planetary Camera. Exceptions include galaxies which depart from pure power-laws at large radius, those with strong nuclear components, and galaxies partly obscured by dust. The uncertainties in the derived parameters are estimated using Monte-Carlo simulations which test the stability of solutions in the face of photon noise and the effects of the deconvolution process. The covariance of the structural parameters is examined by computing contours of constant  $\chi^2$  in multi-dimensional parameter space.

*Subject headings:* galaxies: nuclei - galaxies: elliptical and lenticular, cD

## 1. Introduction

Recent Hubble Space Telescope (HST) observations of early-type galaxies reveal that the central parts have surface-brightness distributions that are different from the extrapolation of traditional fitting formulae derived from ground-based observations (Crane *et al.* 1993; Kormendy *et al.* 1995; van den Bosch *et al.* 1994; Forbes, Franx, & Illingworth 1995, Lauer *et al.* 1995, hereafter Paper I). The surface brightness profiles generally consist of two distinct regions; a steep power-law regime ( $I(r) \propto r^{-\beta}$ ) at large radius, and a shallower power law ( $I(r) \propto r^{-\gamma}$ ) at small radius. Galaxies with a quite shallow inner power-law slope ( $\gamma < 0.3$ ) are classified as “core” galaxies, while those with  $\gamma > 0.5$  are labeled power-law galaxies (Paper I). Note that  $\gamma$  is significantly different from zero in most objects studied with HST thus far, with only rare exceptions (van den Bosch *et al.* 1994; Paper I; Ajhar *et al.* 1995).

Conventional parameters characterizing the luminosity structure of the central regions are the central surface brightness and the core radius, defined as the radius where the surface brightness is half the central value. These parameters have been very useful in understanding elliptical galaxies and bulges of later type galaxies, especially through the fundamental plane correlations (Kormendy 1982, 1984, 1985, 1987a, b; Lauer 1985). However, as we do not find constant surface brightness cores in most HST observations, we set about finding an alternative parameterization (presented below) to better describe the observed surface brightness distributions. For a more detailed history on this subject, readers are referred to Paper I.

An alternative approach to the one taken here is that of Gebhardt *et al.* 1996), who carry out a non-parametric analysis of essentially the same sample considered here. The Gebhardt *et al.* analysis is both more thorough and more accurate, but it largely verifies the simple fits we describe below. The major advantage of the approach taken in the present paper is that it reduces each galaxy to a set of 5 numbers. On the other hand, the non-parametric approach does not force galaxies into possibly ill-fitting boxes.

A one-parameter family of models for spherical stellar systems which yields double power-law surface brightness profiles was introduced independently by Dehnen (1993;  $\gamma$  models) and by Tremaine *et al.* (1994;  $\eta$  models). In the notation of Tremaine *et al.*, the density

$$\rho_\eta(r) \equiv \frac{\eta}{4\pi} \frac{1}{r^{3-\eta}(1+r)^{1+\eta}}, \quad 0 < \eta \leq 3. \quad (1)$$

However, the majority of the actual galaxy profiles is not well-fit by  $\eta$ -models. Although these models allow for a range of inner power-law slopes, the variations apparent in the sharpness of the transition from inner to outer power-laws cannot be reproduced, and the fixed asymptotic outer slope of  $r^{-3}$  does not fit all galaxies.

To parametrize the HST-observed surface brightness profiles, we introduced in Paper I a more general empirical double power-law (the “Nuker” law):

$$I(r) = I_b 2^{\frac{\beta-\gamma}{\alpha}} \left(\frac{r}{r_b}\right)^{-\gamma} \left[1 + \left(\frac{r}{r_b}\right)^\alpha\right]^{-\frac{\beta-\gamma}{\alpha}} \quad (2)$$

The break radius,  $r_b$ , is the radius at which the steep outer profile,  $I(r) \propto r^{-\beta}$ , “breaks” to become the inner shallow profile,  $I(r) \propto r^{-\gamma}$ . More precisely,  $r_b$  is the radius at which the absolute logarithmic curvature in the surface brightness profile,  $|d^2 \log I(r)/d(\log r)^2|$ , is a maximum.  $I_b$  is the vertical scaling parameter and is simply the surface brightness at  $r_b$ . As

shown in Paper I, the parameter  $\alpha$  is necessary to account for the variations in the sharpness of the break.

The Nuker law contains many simpler fitting formulae as special cases;

- The Hubble-Reynolds law (Reynolds 1913; Hubble 1930),

$$I(r) = \frac{I_0 a^2}{(r + a)^2},$$

corresponds to  $\alpha = 1$ ,  $\beta = 2$ ,  $\gamma = 0$ .

- The modified Hubble or analytic King law (Binney & Tremaine 1987),

$$I(r) = \frac{I_0 r_c^2}{r_c^2 + r^2},$$

corresponds to  $\alpha = 2$ ,  $\beta = 2$ ,  $\gamma = 0$ .

- de Vaucouleurs'  $r^{1/4}$  law (de Vaucouleurs 1948),

$$I(r) = I_0 \exp(-kr^{1/m}), \quad m = 4,$$

and its generalization to arbitrary  $m$  (Sersic 1968), corresponds to the parameters  $\alpha = \frac{1}{m}$ ,  $\gamma = 0$ , in the limit  $r_b \rightarrow \infty$ ,  $\beta = \frac{1}{m}kr_b^{1/m} \rightarrow \infty$ .

- Ferrarese et al. (1994) fit HST photometry of early-type galaxies to the law,

$$I(r) = 2^{1/2} I_c \left(\frac{r}{r_c}\right)^{-\beta_1} \left[1 + \left(\frac{r}{r_c}\right)^{2(\beta_2 - \beta_1)}\right]^{-1/2},$$

which corresponds to  $\alpha = 2(\beta_2 - \beta_1)$ ,  $\beta = \beta_2$ ,  $\gamma = \beta_1$ .

Galaxies in which the three-dimensional luminosity density varies smoothly near the center are said to have “analytic cores”. An analytic core requires that the surface brightness near the center has the form  $I(r) = I_0 + I_1 r^2 + O(r^4)$ . Thus only galaxies with  $\alpha = 2$ ,  $\gamma = 0$  have analytic cores.

The Nuker law also provides excellent fits to the family of  $\eta$ -models (Figure 1). The behavior of the five Nuker parameters for each of the  $\eta$ -models is illustrated in Figure 2 in order to show the parameter space occupied by  $\eta$ -models. As will be seen below, real galaxies cover a much wider range in these parameters.

The Nuker law is convenient not only for describing the observed surface brightness distribution but also for computing quantities such as the luminosity density and the local and line-of-sight velocity dispersion distributions. A FORTRAN code that carries out these tasks is available on request from S. Tremaine.

In this paper, we fit the Nuker law and derive the associated structural parameters for 57 early-type galaxies observed with the HST. With the exception of NGC 4881, all objects were observed prior to the HST refurbishment with the Planetary Camera (0.043 per pixel) using filter F555W (corresponding roughly to Johnson  $V$ ). The sample includes early-type galaxies observed as part of our Guest Observer (GO) programs (#2600, #3912, PI Faber), as part of several WFPC Instrument Definition Team programs (#1105, #3229, #3286, #3639, & #5233, PI Westphal), and includes F555W PC images of early-type galaxies publically available in the HST archive by June 23, 1994. The latter were taken as part of GO programs #1038 (PI Ford) and #2607 (PI Jaffe). While small amounts of dust could generally be avoided in determining surface brightness profiles, galaxies with severe nuclear dust obscuration were rejected. Two or more exposures were used for each galaxy to permit cosmic ray rejection, and the peak counts per pixel in the coadded frames were typically  $\sim 2000$  before deconvolution. Further details of data acquisition and reduction of the GO #2600/3912 sample are given in Paper I. These reduction procedures have been uniformly applied to the additional galaxies in the present sample. The only exception is NGC 4881, which was observed after the refurbishment of HST and therefore did not require extensive deconvolution. The parameters determined in this paper are used in the analysis and interpretation of core properties presented in Faber *et al.* (1996, Paper III).

## 2. Fitting Scheme

The five structural parameters are determined using a  $\chi^2$ -minimization method.  $\chi^2$  is defined as the sum of the squares of the differences in surface brightness,  $\Delta\mu(r)^2$ , between the observed profiles and those generated by the Nuker law, where  $\mu(r)$  is in units of magnitudes per arcsecond squared. We make use of the *mean* profiles rather than the major-axis profiles published in Paper I. Each galaxy is fitted with a series of concentric ellipses and the *mean* profile is defined so that for each isophotal ellipse,  $r = \sqrt{r_{maj} \cdot r_{min}}$ , where  $r_{maj}$  and  $r_{min}$  are major and minor axis radii, respectively. The use of mean profiles rather than major-axis profiles reduces the complexities caused by the variation of ellipticity with radius. Significant variations in ellipticity may cause the apparent shape of the major axis and mean surface brightness distributions to differ quite substantially.

As discussed in Paper I, the surface brightness measurements were made using two

procedures, one optimized for high resolution in the inner arcsecond (Lauer 1985) and the other optimized to handle the low signal-to-noise ratio data at larger  $r$ . The two profiles were subsequently combined. However, the resulting profile has inappropriate spacing between data points when plotted in logarithmic space; this is especially true for the profile obtained from the high resolution optimized technique, for which the point spacing is linear. In order to treat all radii with equal importance for our power-law fitting, the observed profiles were resampled beginning at the first measured data point ( $0.044''/\sqrt{2\pi} = 0.017''$ ) and progressing at equal logarithmic intervals of  $\Delta \log r = 0.05$  using spline interpolation. This spacing is small enough to represent the variation of surface brightness in the original profiles. Uniform weights and errors were applied to the individual data points in the resampled profile during the fitting procedure.

For the minimization we have used the MINUIT package, which handles non-linear minimization through a combination of Monte-Carlo search, downhill-Simplex, and the variable metric method (James and Roos 1977). Due to the optical problems inherent in pre-refurbishment HST data and the high central concentration of light in the galaxies themselves, we applied the following additional adjustments to the minimization procedure.

Even with an accurate point-spread function (PSF) and careful image deconvolution, the effect of the spherical aberration of the HST primary cannot be completely corrected within  $0.''1$  of the galaxy centers (Lauer *et al.* 1992b). Therefore the fitting domain is restricted to radii greater than  $0.''1$ . Nevertheless profiles do differ greatly within  $0.''1$ , so there is some information there. To utilize this, the *total light* within  $0.''1$  (as opposed to its distribution) was used as an additional constraint on the the fit. The weight of the central light is equivalent to the sum of weights for the resampled data points which lie within  $0.''1$ . Note that the constraint given by the central light does not necessarily force the fit to pass through the data points within  $0.''1$ . Large departures between the fit and the innermost data point often occur. This is because the total light is easily adjusted by only a slight change in the surface brightness in the outer region (but still within  $0.''1$ ), where the areal coverage is comparatively large.

Nuker law fits to the sample galaxies are shown in Figure 3, and the structural parameters are listed in Table 1. For a few galaxies with nuclei such as NGC 1331, NGC 3599, and NGC 4239, a separate fit was made to the bulge component only, excluding the nucleus. In these cases, the central light constraint is also ignored in the fit. Any dust patches were masked out from the raw image before the profile extraction. Nevertheless the galaxies with significant dust features, such as NGC 524, show distinct distortions in their profiles. In these cases, we set the weights to zero in the regions obviously affected by dust obscuration. For each galaxy, the fitting domain is shown by the solid symbols. The RMS deviation

computed over the fitting domain between the model and the original surface brightness measurements is listed in Table 1.

While the Nuker fits generally match quite well the observed profiles out to the outermost HST data points ( $r \sim 10''$ ), there are cases like Abell 1020, NGC 4478, and NGC 4486B, where the outer parts deviate (both upward and downward) from the Nuker law. Even galaxies which show good agreement with the Nuker law within  $10''$  in general will also fail at much larger radii beyond the field covered by the present HST data, as the profiles follow a curving de Vaucouleurs law, not a power law there. For some of the sample galaxies, the HST data are combined with ground based photometry covering much larger area and presented in Kormendy *et al.* (1996, in preparation).

### 3. Parameter Uncertainties

#### 3.1. Error Estimates

The deconvolution process can introduce systematic errors into surface-brightness profiles, particularly if use is made of an inappropriate PSF. Experiments with different PSFs were carried out in Paper I and revealed both photometric offsets and changes in slope out to  $\sim 2''$ . These effects are more pronounced for galaxies with steep surface brightness profiles near the center. However, the experiments showed that even for galaxies with particularly sharp nuclei, the systematic errors in the inner parts (where the effects of deconvolution are greatest) are small ( $\sim 0.^m06$ ). We note that the slope change would be echoed primarily by  $\gamma$ ,  $\alpha$ , and  $I_b$ ;  $\beta$  and  $r_b$  would be essentially unaffected.

The deconvolution process also amplifies photometric uncertainties, and we have carried out simulations to better understand the errors in the Nuker parameters introduced by deconvolution of data with a finite signal-to-noise ratio. Each simulation was carried out as follows: (i) Poisson noise appropriate to the number of collected photons in each pixel was added to the raw (undeconvolved) image of a galaxy. (ii) Each such realization was deconvolved using 80 iterations of the Lucy-Richardson deconvolution algorithm. (iii) The two-dimensional data were fitted with a series of concentric ellipses as described in Paper I. (iv) The mean profiles were fitted with the Nuker law and the resulting parameters stored.

It is important to note that we have added artificial noise on top of the natural noise already present in the data. In this sense, our simulations *overestimate* (by  $\approx \sqrt{2}$ ) the errors due purely to S/N. To isolate the effects of S/N alone, we generated a noiseless model image and repeated the experiments. By comparing the results of these experiments to those using real data, we were able to estimate to what extent the goodness of fit was determined by

non-photon statistical errors, such as changes in ellipticity, flat-field defects, unsubtracted stars, undetected dust obscuration, *etc.*

We chose three galaxies for this exercise : Abell 1831, NGC 4889, and NGC 4434. Abell 1831 and NGC 4889 are typical examples of well resolved core galaxies with small  $\gamma$ , while NGC 4434 is a power-law galaxy. These galaxies also span a large range in central signal-to-noise ratio. Abell 1831 has the lowest central signal-to-noise ratio in the sample, with a peak data count around  $1.0 \times 10^3$ DN (digital numbers) per pixel. By comparison, NGC 4889 has a peak count of  $6.9 \times 10^3$ DN per pixel, and NGC 4434 has a peak count of  $1.1 \times 10^4$ DN per pixel.

For each galaxy one hundred realizations of the original image were generated. These realizations were then deconvolved and independently analyzed. We constructed a symmetric, two-dimensional, noiseless model image based on the best-fit parameters for Abell 1831, convolved with an appropriate PSF, and scaled to match the signal-to-noise ratio in the real image. Experiments with this model image provided a worst-case upper limit on the degree to which the results in Table 1 are affected by purely statistical uncertainties.

The profiles fitted to the deconvolved, simulated images are shown in Figure 4. As expected, Abell 1831 and its model representation show the largest spread among the three galaxies, and deviations from the best-fit profile are apparent out to  $r \sim 1''$ . NGC 4889 also shows an obvious dispersion, but in this case the deviations are generally confined to  $r < 0.''1$ , and the fit parameters are rarely significantly different from their best-fit values. NGC 4434 has the highest signal-to-noise ratio and, despite the steepness of the profile near the center, the effects of photon noise and deconvolution appear to be minimal.

We note that deconvolving a natural image with added noise changes the shape of the simulated profiles somewhat, at least in the case of Abell 1831 and its model representation. There is a slight increase in surface brightness in the region  $0.''1 < r < 1''$ . The Nuker parameters derived from the simulated profiles therefore are somewhat different from those listed in Table 1. This effect is not detected in the other two galaxies with higher signal-to-noise ratios, and we attribute it to the non-conservative nature of the Lucy-Richardson deconvolution algorithm employed.

The frequency distributions of the best-fit Nuker parameters for the four galaxy images are plotted in Figure 5. The mean parameter value and associated standard deviation in each panel were determined by fitting a Gaussian to each frequency histogram. As expected from the amplitude of the variations apparent in the simulated profiles, Abell 1831 shows the largest standard deviation for each of its Nuker parameters except  $\beta$ .  $\beta$ , the slope of the outer power-law, is rather stable in Abell 1831 because  $r_b$  is comparatively small and the



outer power law portion of the profile is sampled over a large radial range.

The average values of the Nuker parameters for Abell 1831 and its model representation are also not identical. This is due in part to the different noise characteristics of the two images near the break radius and their amplification in the deconvolution process. It is also due to the fact that the model image does not exactly mimic the real data. For example, the slight dip apparent at  $r \sim 0.''15$  in the real data is not reproduced in the model image, and the best fits will differ accordingly.

We note that there is no significant difference in  $\chi^2$  between the best-fit Nuker parameters for Abell 1831 and those for its noiseless model representation. This implies that our computed  $\chi^2$  is much less dependent on signal-to-noise ratio than it is on other factors. These factors would include image defects as well as real discrepancies in form between Nuker profiles and those of galaxies.

In spite of its low signal-to-noise ratio, both Abell 1831 and its model representation show that errors in the Nuker parameters introduced by photon noise and deconvolution are small. We conclude that the entries in Table 1 are largely unaffected by differences in signal-to-noise ratio.

### 3.2. Covariances

The uncertainties in the derived parameters and the coupling of the parameters with one another are usually investigated using the distribution of  $\chi^2$ . For any two parameters, we can project the 5-dimensional  $\chi^2$  distribution onto the appropriate axes. This reveals not only the how individual parameters are constrained by the data, but also the degree to which various parameters are correlated. However, since the data have been resampled and assigned uniform weights in order to put equal emphasis on different portions of the surface brightness profiles, the values of  $\chi^2$  we compute, while relatively correct, are not properly normalized to compute absolute uncertainties. Our use of the total light within  $0.''1$  as an arbitrarily weighted, additional constraint exacerbates this problem. We could conceivably compute an *a priori*  $\chi^2$  based on photon statistics, but that would not include errors due to flat-fielding defects, improper deconvolution, and systematic mismatch between the Nuker law and the galaxies.

In Figure 6 we show projected, constant- $\chi^2$  contours for several combinations of Nuker parameters for the three galaxies considered in the previous section. For the reasons given above, the confidence limits for each parameter cannot be directly estimated from the initially computed  $\chi^2$  values. To remedy this, we have normalized the computed  $\chi^2$  values using the

observed distributions of best-fit parameters found in the Monte Carlo simulations. The inner, thick contours in Figure 6 thus correspond to the  $1\sigma$  errors determined from the Monte Carlo simulations. In order to show the gradient of the projected  $\chi^2$  distribution, the outer, thick contours are used to indicate the  $10\sigma$  level. This Monte Carlo normalization includes photon statistics but not the other error sources noted above, so the treatment is approximate.

The general conclusion from these plots is that, while certain error pairs are correlated, the only truly serious correlation is between  $r_b$  and  $\mu_b$  for power law galaxies. This is to be expected, as these parameters are formally completely unconstrained for pure power laws with zero curvature.

If we exclude those galaxies with nuclei (NGC 1331, 3599, 4239, and 6166) or with obvious and widespread dust (NGC 524), the remaining 52 galaxies give a mean RMS deviation between the best-fit Nuker law and the surface brightness measurements of 2.7% (0.03 mag). This is comparable to, though somewhat larger than, an RMS of 1% obtained by Gebhardt *et al.* (1996) using smoothed spline fits to the data. This simply reflects the fact that the Nuker law is a smoother estimate of the surface brightness compared with the non-parametric fit. For the purposes of determining the physical properties of an individual galaxy, it is therefore preferable to invert a non-parametric form of the surface brightness profile. However, if one is searching for global trends and systematics, the Nuker parameters provide a convenient basis for comparison. The conclusions reached in Paper I and Faber *et al.* (1996) based on the Nuker parameters are not altered with the application of non-parametric methods.

#### 4. Summary

In this paper, we derive a set of structural parameters for 57 early-type galaxies observed with HST. These parameters are based on the empirical “Nuker” law, which successfully describes the central surface-brightness distributions within the radius range from  $\sim 0.1''$  to  $\sim 10''$  for most galaxies in the sample. These parameters have been used in Paper I and Faber *et al.* (1996) to identify distinct classes of objects, characterized by significant differences in one or more of the Nuker parameters. While these parameters can in principle also be used to evaluate luminosity densities and (with the availability of suitable spectral information) the run of velocity dispersion with radius, we believe this would be better left to non-parametric methods (Gebhardt *et al.* 1996), which are more faithful to small but significant undulations in the observed profiles.

This research was supported in part by NASA grant GO-02600.01-87A.

## REFERENCES

- Ajhar, E. A. *et al.* 1996, in preparation
- Binggeli, B., Sandage, A., & Tammann, G. A. 1985, *AJ*, 90, 1681
- Binney, J., & Tremaine, S. 1987, in *Galactic Dynamics* (Princeton University Press, Princeton), p. 230
- Crane, P. *et al.* 1993, *AJ*, 106, 1371
- Dehnen, W. 1993, *MNRAS*, 265, 250
- de Vaucouleurs, G. 1948 *Ann. d'Astrophys.*, **11**, 247
- Faber, S. M. *et al.* 1996, in preparation (Paper III)
- Ferrarese, L., Van den Bosch, F. C., Ford, H. C., Jaffe, W., & O'Connell, R. W. 1994, *AJ*, 108, 1598
- Forbes, D. A., Franx, M., & Illingworth, G. D. 1995, *AJ*, 109, 1988
- Gebhardt, K., Richstone, D., Ajhar, E.A., Lauer, T.R., Byun, Y.I., Kormendy, J., Dressler, A., Faber, S.M., Grillmair, C., & Tremaine, S. 1996, *AJ*, in press.
- Hubble, E. P. 1930, *ApJ*, 71, 231
- James, F. & Roos, M. 1977, CERN/D internal report 77/506
- Kormendy, J. 1982, in *Morphology and Dynamics of Galaxies*, ed. L. Martinet & M. Mayor (Sauverny: Geneva Observatory), p. 113
- Kormendy, J. 1984, *ApJ*, 287, 577
- Kormendy, J. 1985, *ApJ*, 295, 73
- Kormendy, J. 1987a, in *IAU Symposium 127, Structure and Dynamics of Elliptical Galaxies*, ed. T. de Zeeuw (Dordrecht: Reidel), p. 17
- Kormendy, J. 1987b, in *Nearly Normal Galaxies: From the Planck Time to the Present*, ed. S.M. Faber (New York: Springer), p. 163
- Kormendy, J., Dressler, A., Byun, Y. I., Faber, S. M., Grillmair, C., Lauer, T. R., Richstone, D. O., & Tremaine, S. 1994, in *ESO/OHP Workshop on Dwarf Galaxies*, ed. G. Meylan & P. Prugniel (Garching:ESO), p.147
- Kormendy, J. *et al* 1996, in preparation
- Lauer, T.R. 1985, *ApJ*, 292, 104
- Lauer, T. R., Faber, S. M., Lynds, C. R., Baum, W. A., Ewald, S. P., Groth, E. J., Hester, J. J., Holtzman, J. A., Kristian, J., Light, R. M., O'Neil Jr, E. J., Schneider, D. P., Shaya, E. J., & Westphal, J. A. 1992a, *AJ*, 103, 703

- Lauer, T. R., Faber, S. M., Currie, D. G., Ewald, S. P., Groth, E. J., Hester, J. J., Holtzman, J. A., Light, R. M., O’Neil Jr, E. J., Shaya, E. J., & Westphal, J. A. 1992b, AJ, 104, 552
- Lauer, T. R., Ajhar, E. A., Byun, Y. I., Dressler, A., Faber, S. M., Grillmair, C., Kormendy, J., Richstone, D., & Tremaine, S. 1995, AJ, 110, 2622 (Paper I)
- Reynolds, J.H. 1913, MNRAS, 74, 132
- Sersic, J.L. 1968, AJ, 73, 892
- Tremaine, S., Richstone, D. O., Byun, Y. I., Dressler, A., Faber, S. M., Grillmair, C., Kormendy, J., & Lauer, T. R. 1994, AJ, 107, 634
- van den Bosch, F. C., Ferrarese, L., Jaffe, W., Ford, H. C., & O’Connell, R. W. 1994, AJ, 108, 1579

Fig. 1.— Surface brightness profiles for  $\eta$ -models with a range of  $\eta$  values (*open circles*). Solid line represents Nuker law fits to each model profile.

Fig. 2.— Nuker parameters for  $\eta$  models. Left diagrams are for the fits made to the radius range from  $10^{-5}$  to  $10^3$ . Right diagrams are with the restricted radius range of  $0.1 < r < 10$ , which is comparable to our fitting regime for the sample galaxies.  $\mu_b$  is the surface brightness at  $r_b$ , *i.e.*  $\mu_b = -2.5 \log_{10} I_b$ .

Fig. 3.— Mean surface brightness profiles (*filled and open circles*) and Nuker law fits (*solid lines*) for the sample galaxies. The surface brightness is in  $mag/sec^2$ . The filled circles indicate the domain over which the fits are were computed, while the open circles denote the points excluded from the fit. The data points inside  $r \sim 0.''1$  are regarded as uncertain, therefore are not directly used in the fitting (see text).

Fig. 4.— Simulated surface brightness profiles (*solid lines*) for Abell 1831, NGC 4889 and NGC 4434, shown with the original profile (*open circles*). The top diagram is for the noiseless model image of Abell 1831. The peak data counts are  $1.0 \times 10^3$ DN for Abell 1831,  $6.9 \times 10^3$ DN for NGC 4889, and  $1.1 \times 10^4$ DN for NGC 4434 respectively. The means and RMSs of the numerical experiments at  $0.''03$  and  $0.''05$  are shown as open squares with error bars.

Fig. 5.— Frequency histogram of Nuker parameters derived from 100 simulated profiles of the noiseless model image of Abell 1831, Abell 1831, NGC 4889, and NGC 4434. A Gaussian distribution is evaluated for each parameter and shown by solid curve. The mean and standard deviation values are given.  $\mu_b$  is in  $mag/sec^2$  and  $r_b$  is in arcsec.

Fig. 6.— Parameter cross-correlations shown by the  $\chi^2$  ellipses for Abell 1831, NGC 4434, and NGC 4889.  $\mu_b$  is in  $mag/sec^2$  and  $r_b$  is in arcsec. The thick solid curves indicate  $1\sigma$  and  $10\sigma$  ellipses as scaled by the results of Monte-Carlo simulations given in Figure 5. The locations of the minimum  $\chi^2$  are indicated by crosses.

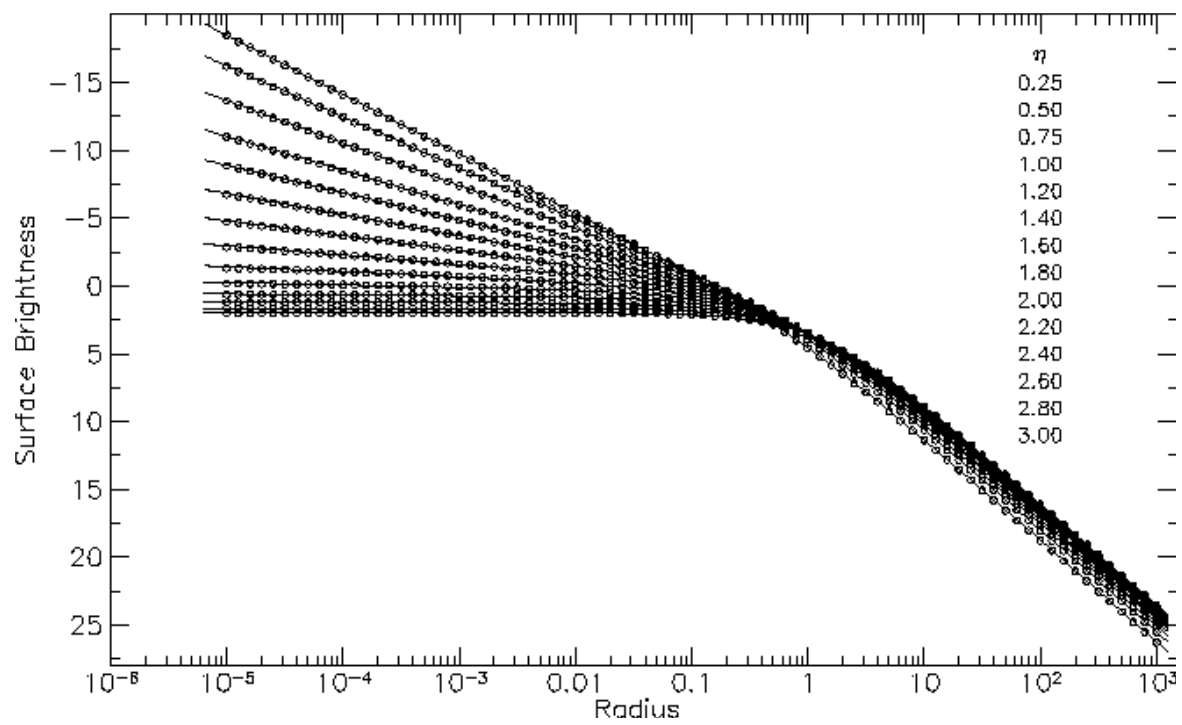


TABLE 1 : STRUCTURAL PARAMETERS

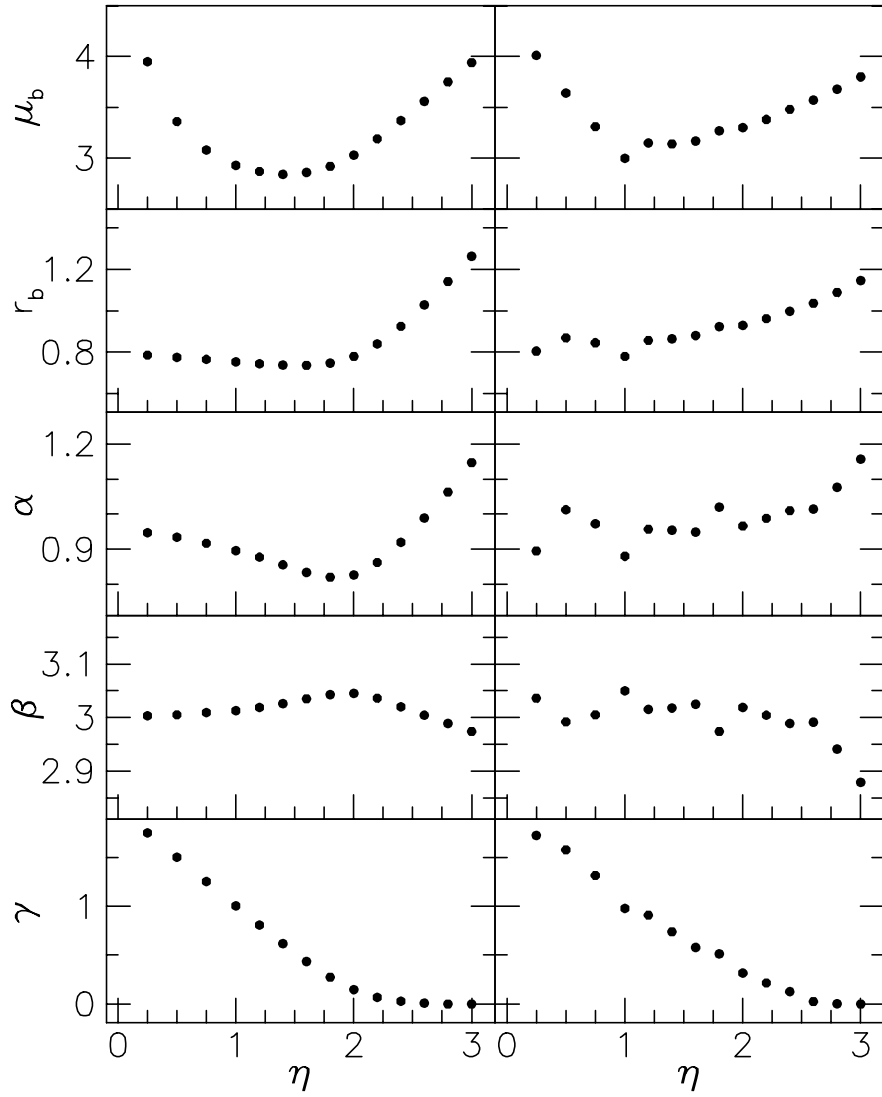
Galaxy	Sample	$\mu_b^\dagger$	$r_b$	$\alpha$	$\beta$	$\gamma$	RMS (%)	Note
Abell 1020	3912	17.160	0.236	2.564	1.394	0.175	1.34	
Abell 1831 $\ddagger$	2600	18.698	0.500	3.567	1.170	0.110	2.19	
Abell 2052	2600	18.600	0.419	8.022	0.749	0.201	3.71	nuclear point source excluded in fit
NGC 524	3912	16.121	0.322	1.293	1.001	0.005	5.36	dust region excluded in fit
NGC 596	2600	18.116	3.501	0.758	1.968	0.554	3.37	
NGC 720	2600	17.500	3.208	2.315	1.660	0.062	0.51	
NGC 1023	2600	16.357	1.865	4.722	1.184	0.782	2.28	
NGC 1172	3912	18.694	2.431	1.517	1.638	1.009	3.43	
NGC 1331	3912	21.035	8.157	1.378	2.842	0.472	2.22	nucleus excluded in fit ("bulge")
NGC 1331	3912	19.976	4.083	4.470	1.615	0.673	5.76	nucleus included in fit
NGC 1399	2600	17.059	3.144	1.504	1.682	0.068	0.70	
NGC 1400	3912	15.510	0.330	1.395	1.319	0	3.20	
NGC 1426	3912	17.540	1.644	3.619	1.354	0.847	3.06	
NGC 1600	3639	18.951	5.133	1.255	2.177	0	2.27	
NGC 1700	3912	14.041	0.088	0.903	1.303	0	2.39	
NGC 2636	3912	15.708	0.093	1.838	1.140	0.042	3.11	
NGC 2832	3912	17.452	0.910	1.837	1.399	0.024	1.05	
NGC 2841	3912	14.548	0.133	0.928	1.021	0.009	3.55	
NGC 3115	2600	16.248	2.906	1.466	1.429	0.791	1.59	
NGC 3377	2600	12.902	0.089	1.923	1.332	0.292	2.71	
NGC 3379	3229	16.136	1.738	1.593	1.432	0.182	2.05	
NGC 3599	3912	17.390	1.219	13.760	1.670	0.580	7.43	nucleus excluded in fit ("bulge")
NGC 3599	3912	17.578	1.351	13.009	1.660	0.794	9.12	nucleus included in fit
NGC 3605	2600	17.253	0.886	9.135	1.263	0.671	2.15	
NGC 3608	3912	15.449	0.284	1.052	1.330	0	1.55	
NGC 4168	2607	18.357	2.521	0.945	1.500	0.140	1.55	
NGC 4239	3912	18.028	0.815	4.237	0.967	0.352	3.20	nucleus excluded in fit ("bulge")
NGC 4239	3912	18.420	1.284	14.531	0.959	0.646	7.81	nucleus included in fit
NGC 4258	1038	13.712	0.046	1.047	0.873	0.002	3.74	
NGC 4365	2607	15.448	1.671	2.056	1.270	0.148	1.72	
NGC 4387	2600	18.993	4.423	3.362	1.591	0.719	2.51	
NGC 4434 $\ddagger$	2600	17.342	1.230	2.809	1.385	0.799	2.86	
NGC 4458	2600	14.541	0.118	5.265	1.427	0.490	2.88	
NGC 4464	2600	17.348	1.212	1.642	1.683	0.884	1.95	
NGC 4467	2600	19.982	3.243	7.518	2.133	0.981	5.68	
NGC 4472	3229	16.659	2.398	2.031	1.165	0.039	1.31	
NGC 4473	2607	17.335	3.704	0.665	2.447	0.014	1.92	double nucleus?
NGC 4478	2607	15.458	0.175	3.321	0.836	0.427	2.54	
NGC 4486	1105	17.923	7.606	2.816	1.394	0.246	0.62	point source removed; profile from Lauer <i>et al</i> (1992a)
NGC 4486B	3912	14.976	0.181	2.781	1.329	0.139	1.23	
NGC 4551	2600	18.922	3.862	2.944	1.233	0.802	2.65	
NGC 4552	3286	15.512	0.649	1.483	1.297	0	4.37	
NGC 4564	2607	15.722	0.516	0.255	1.905	0.047	3.35	
NGC 4570	2607	17.292	2.819	3.715	1.491	0.845	2.31	
NGC 4621	3229	17.250	2.922	0.187	1.710	0.496	3.15	
NGC 4636	3912	17.732	3.213	1.644	1.329	0.129	1.36	
NGC 4649	3229	17.191	3.584	2.005	1.300	0.153	2.62	
NGC 4697	3912	16.957	2.575	24.863	1.040	0.742	4.12	dust disk excluded from fit
NGC 4742	2600	16.764	1.386	48.599	1.994	1.091	4.64	
NGC 4874	3912	19.222	2.632	2.327	1.366	0.134	1.23	
NGC 4881	5233	17.330	0.498	1.763	1.358	0.757	3.25	post refurbishment data
NGC 4889 $\ddagger$	3912	18.053	1.675	2.613	1.348	0.047	1.26	
NGC 5813	3912	16.529	0.792	2.147	1.326	0.076	1.66	
NGC 5845	2600	17.625	2.273	1.266	2.742	0.515	7.61	
NGC 6166	3912	19.348	2.221	3.320	0.992	0.081	1.18	nuclear point source excluded in fit
NGC 7332	2600	15.803	0.767	4.250	1.343	0.897	3.24	
VCC 1199	2600	19.677	1.500	7.986	1.619	1.129	3.99	VCC galaxies from Binggelli <i>et al</i> (1985)
VCC 1440	2600	19.994	2.522	5.537	1.583	0.964	5.17	
VCC 1545	2600	19.710	1.205	7.652	1.018	0.625	4.69	
VCC 1627	2600	20.153	2.989	2.123	2.099	0.948	2.37	

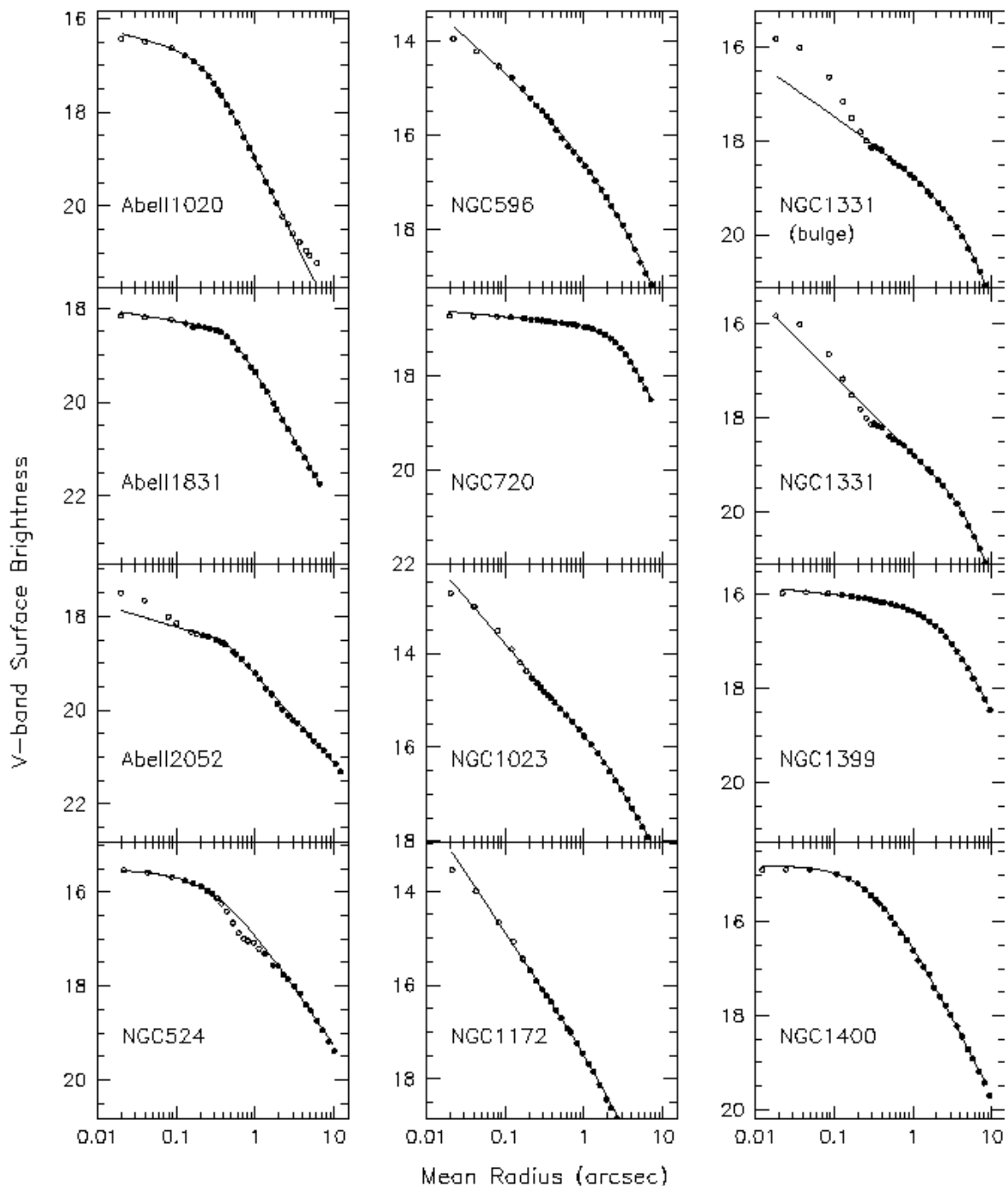
 $\dagger \mu_b = -2.5 \log_{10} I_b$  ; mag/arcsec<sup>2</sup> $\ddagger$  galaxies used for detailed analysis in this paper

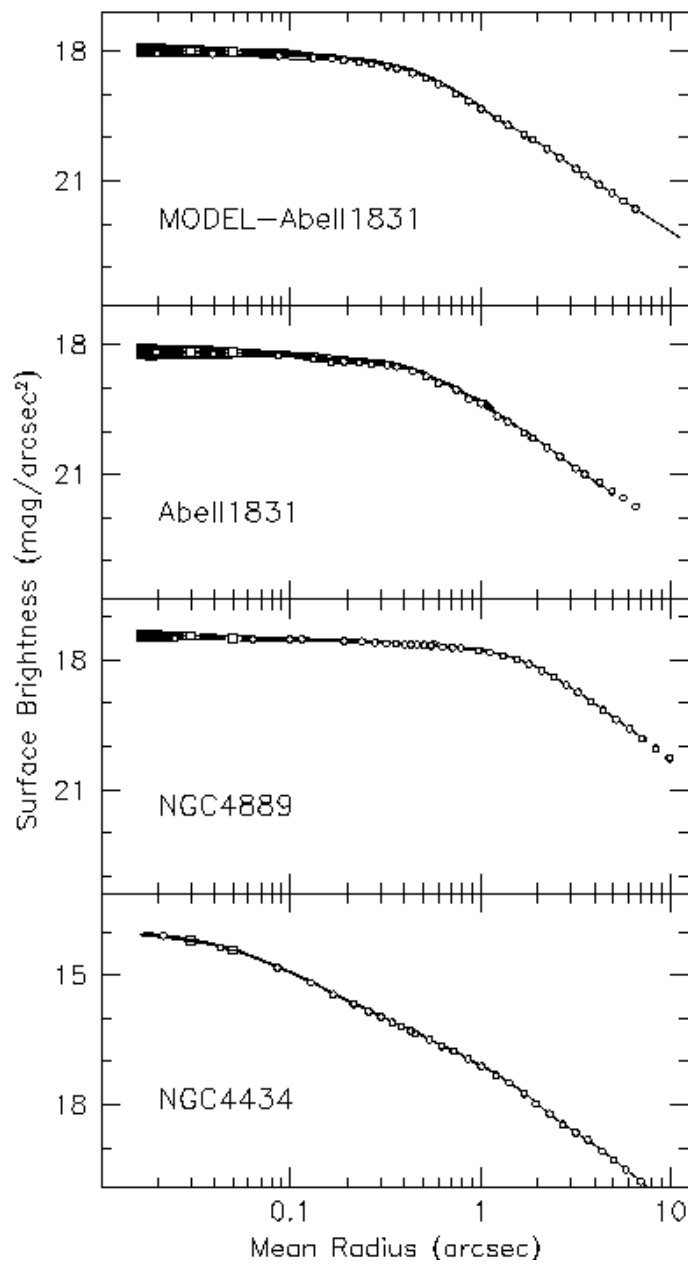


$10^{-5} < r < 10^3$

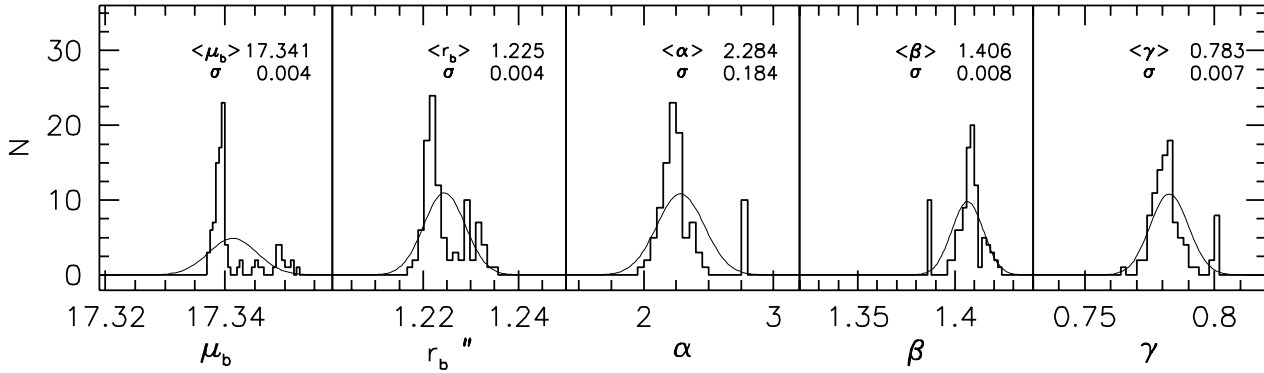
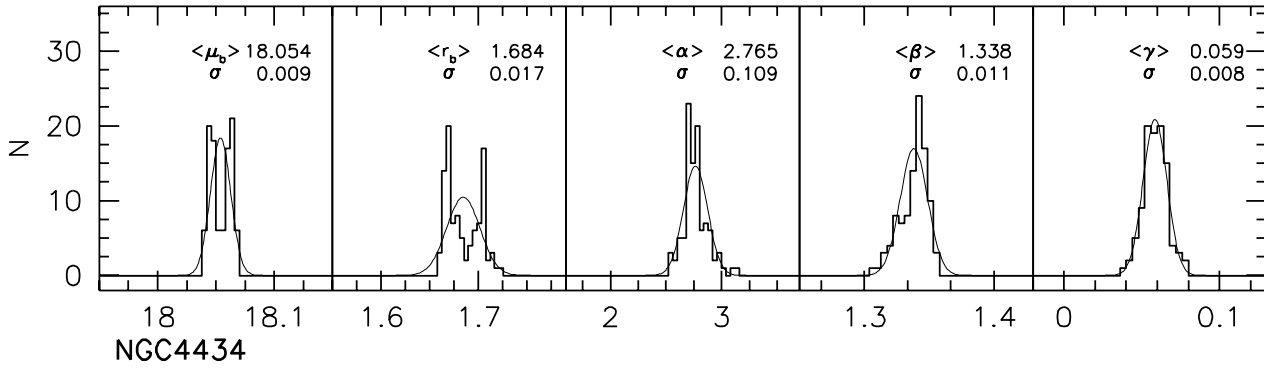
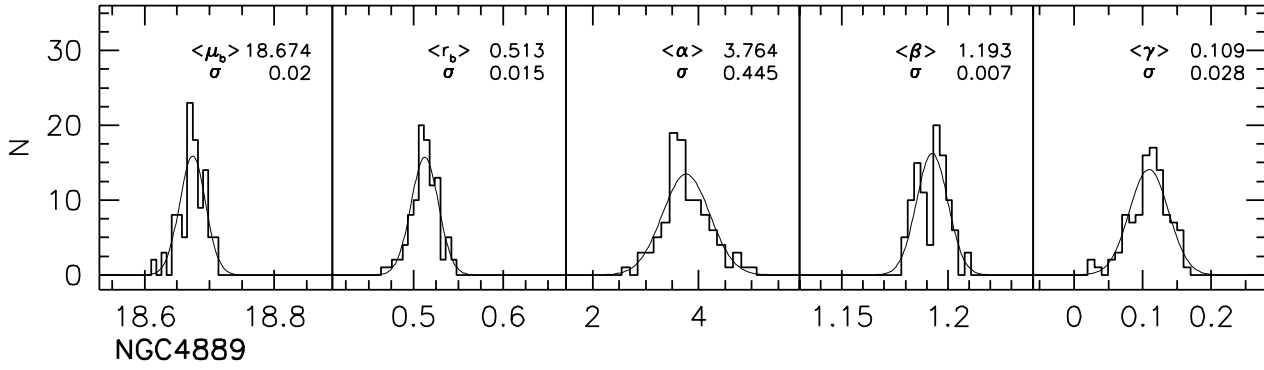
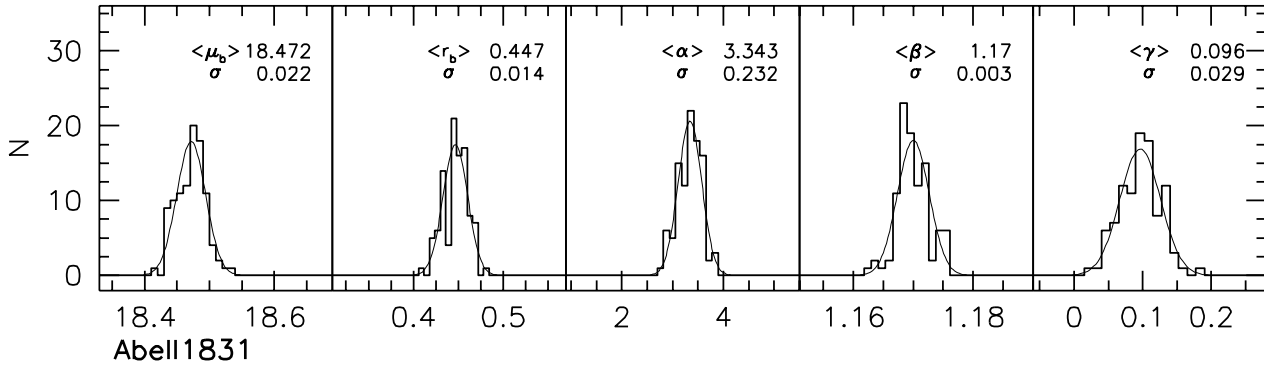
$0.1 < r < 10$



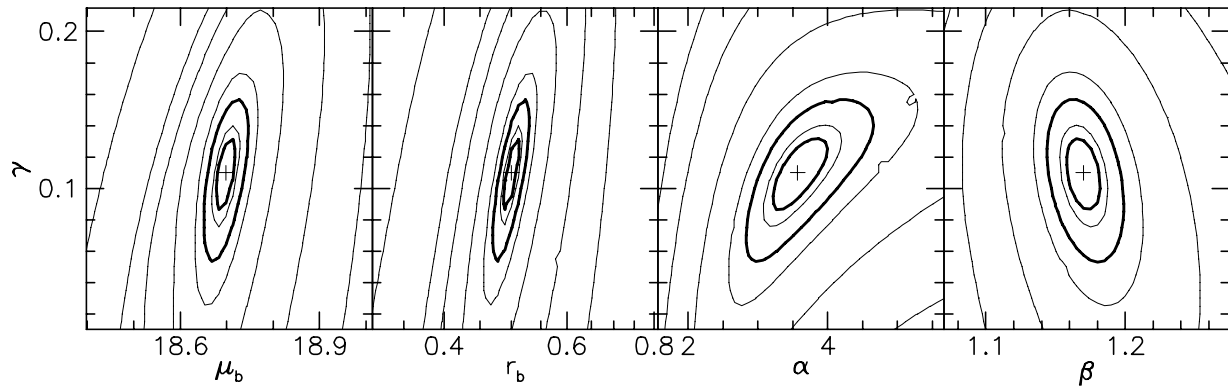
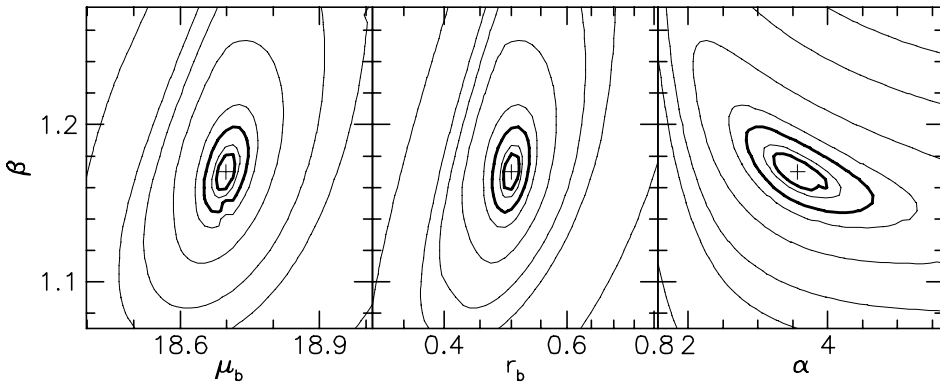
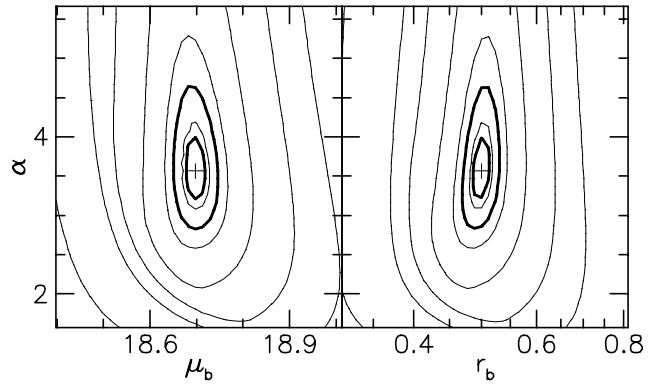
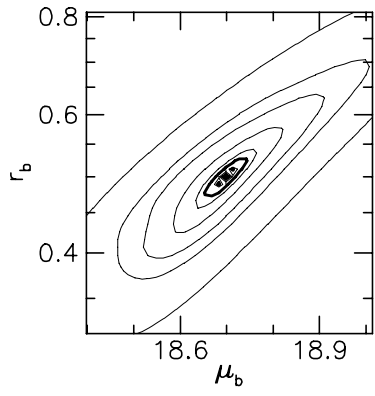




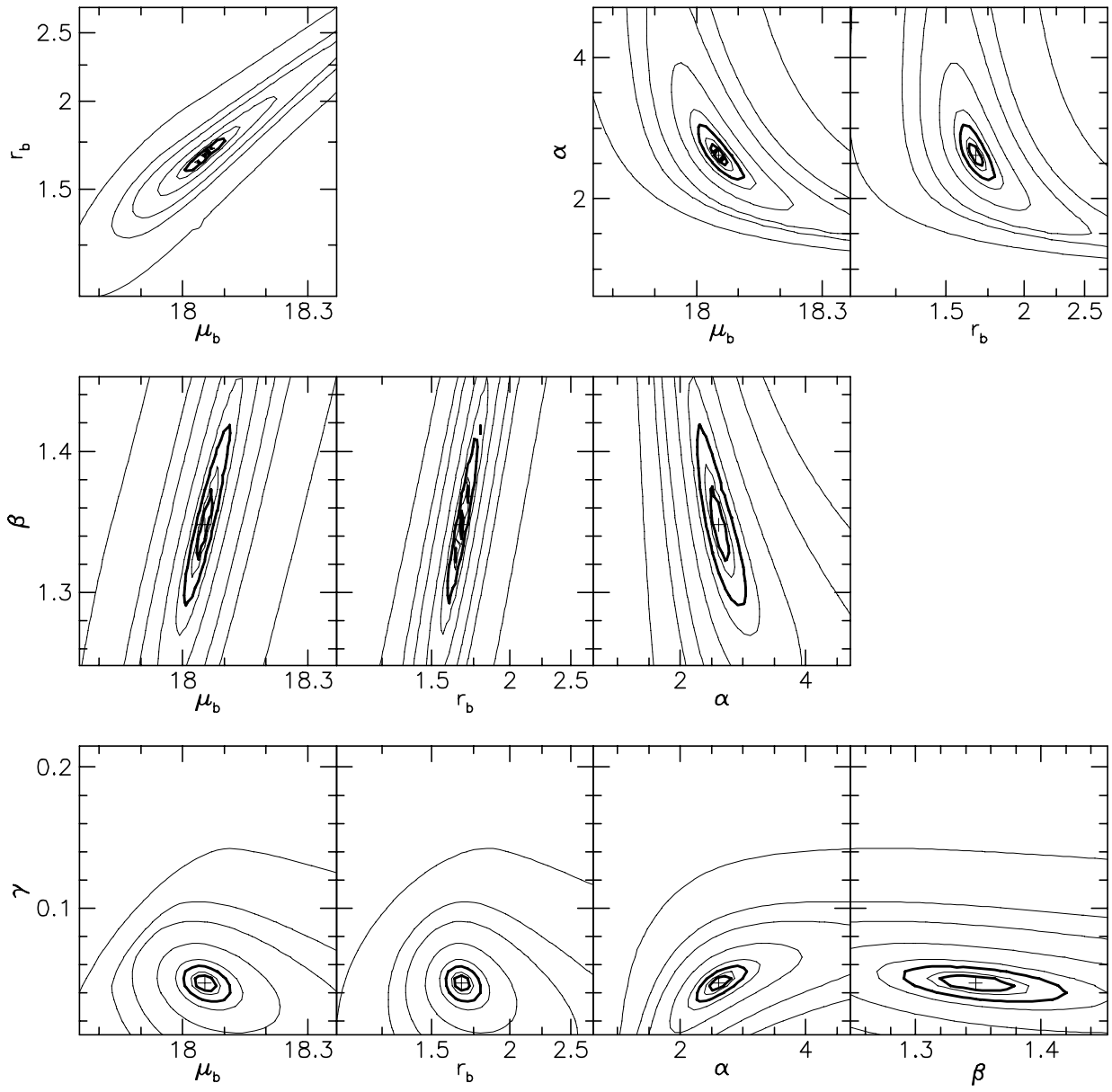
MODEL-Abell1831



Abell1831



NGC4889



NGC4434

